

Surface Wetting of Liquid Nanodroplets: Droplet Size Effects

David R. Heine, Gary S. Grest, Edmund B. Webb III

Sandia National Laboratories, Albuquerque, New Mexico 87185

(Dated: 13th November 2018)

Abstract

The spreading of liquid nanodroplets of different initial radii R_0 is studied using molecular dynamics simulation. Results for two distinct systems, Pb on Cu(111), which is non-wetting, and a coarse grained polymer model, which wets the surface, are presented for Pb droplets ranging in size from $\sim 55\,000$ to $220\,000$ atoms and polymer droplets ranging in size from $\sim 200\,000$ to $780\,000$ monomers. In both cases, a precursor foot precedes the spreading of the main droplet. This precursor foot spreads as $r_f^2(t) = 2D_{eff}t$ with an effective diffusion constant that exhibits a droplet size dependence $D_{eff} \sim R_0^{1/2}$. The radius of the main droplet $r_b(t) \sim R_0^{4/5}$ in agreement with kinetic models for the cylindrical geometry studied.

Numerous practical problems are determined by the wetting of surfaces by liquids including adhesion, lubrication, coatings, plant protection, and oil recovery. The spreading of a droplet on a surface proceeds as the droplet balances the interfacial tensions between the solid, liquid, and vapor phases. Completely wetting droplets are known to form a monolayer film or precursor foot on the surface that spreads ahead of the droplet. For “high-energy” surfaces, spreading includes the formation of molecule-sized terraces along with the precursor foot [1, 2].

Although the spreading behavior of droplets on surfaces has been extensively studied, droplet size effects on the spreading dynamics are often ignored. These size effects can have a large influence on the wetting behavior, particularly when using nanoscale droplets such as in MEMS and microfluidic devices. For these devices, droplet size can strongly affect both the manufacturing speed, such as in microcontact printing, and the device performance.

For a spreading liquid droplet, the energy dissipation mechanics have been classified by de Gennes. The total dissipation in the spreading droplet can be expressed as a sum of three distinct dissipation mechanisms, $T\Sigma_w + T\Sigma_f + T\Sigma_l$ [3]. In this equation, $T\Sigma_w$ is the contribution due to viscous dissipation in the bulk of the droplet, $T\Sigma_f$ is the contribution due to viscous dissipation in the precursor foot, and $T\Sigma_l$ is the contribution due to adsorption of liquid molecules to the surface at the contact line. The adsorption mechanism is expected to dominate for low viscosity systems at short times while the bulk viscous dissipation mechanism takes over at later times [4]. The dissipation from the foot is less understood, though in the simulations presented here we will show that this dissipation does not play a role in the spreading of the droplet.

The size dependence of the bulk droplet spreading rate is present in models of droplet spreading. In the molecular kinetic theory of liquids [5, 6], the energy dissipation occurs at the contact line. In the linearized version of this model, the contact radius $r_b(t)$ of the bulk region of the droplet scales with the droplet volume according to $r_b(t) \sim R_0^{6/7}$ at late times for spherical droplets [7] and $r_b(t) \sim R_0^{4/5}$ for cylindrical droplets [8]. The hydrodynamic model [9, 10] is based upon the solution of the equations of motion and continuity for the droplet and assumes that energy dissipation occurs via viscous dissipation in the bulk. For the hydrodynamic model, the contact radius of the bulk region scales according to $r_b(t) \sim R_0^{9/10}$ at late times for spherical droplets [7] and $r_b(t) \sim R_0^{6/7}$ for cylindrical droplets [8]. de Ruijter *et al.* [7] derived a combined model by including the energy dissipation mechanisms from

both the linearized kinetic and hydrodynamic models. This model does not consider the viscous dissipation in the precursor foot. For a cylindrical droplet, the combined spreading model is [8]

$$\frac{dr_b(t)}{dt} = \frac{\gamma}{\frac{\zeta_0}{2} + \frac{2\eta(r_b(t)-a)\sin^2\theta}{r_b(t)(\theta-\sin\theta\cos\theta)}} \left(\frac{\theta}{\sin\theta} - \frac{\theta_0}{\sin\theta_0} \right), \quad (1)$$

$$\frac{d\theta}{dt} = \left(\frac{\theta - \sin\theta\cos\theta}{A} \right)^{1/2} \left(\cos\theta - \frac{\sin^3\theta}{\theta - \sin\theta\cos\theta} \right)^{-1} \frac{dr_b(t)}{dt}. \quad (2)$$

where the cross-sectional area $A \sim R_0^2$, γ is the liquid/vapor surface tension, ζ_0 is the friction coefficient, η is the bulk fluid viscosity, a is the hydrodynamic cutoff, and θ_0 is the equilibrium contact angle. The linearized kinetic and hydrodynamic models are obtained from Eq. 1 by setting η and ζ_0 to zero, respectively. Although this produces the linearized version of Blake’s kinetic model, experiments [7, 11, 12] and simulation [8, 13, 14, 15] have shown that it works quite well. These models are written for droplets with a finite θ_0 , but they can also be applied to wetting droplets by setting $\frac{\theta_0}{\sin\theta_0} = 1$ in Eq. 1.

Droplets often spread by extending a precursor foot ahead of the main droplet. This has been observed in experiments [3, 16, 17] as well as simulation [8, 13, 18, 19]. This foot grows diffusively, though to the best of our knowledge there are no predictions for the dependence on the droplet size. Droplet spreading experiments have observed “terraced spreading” where multiple layers spread on top of the precursor foot. In simulations of droplet spreading, the precursor foot is present, but terraced spreading has not been observed. This is probably due to the relatively short duration of the simulation runs.

Although droplet size effects are often ignored when studying spreading dynamics, we show that the spreading rate of both the precursor foot and the bulk change with droplet size. Here, we present MD simulations for two very different systems, a coarse-grained model of polymer nanodroplets in the wetting regime and an explicit atom model of Pb on Cu(111), which is non-wetting, to study the dependence of the spreading rate of both the droplet and the precursor foot on the initial radius R_0 of the droplet. Our results demonstrate that the observed behavior is a general phenomenon and does not depend on the system specifics. In both cases, the vapor pressure is low so that spreading does not occur via vaporization and condensation.

For polymer chains, the polymer is represented by spherical beads of mass m attached

by springs, which interact with a truncated Lennard-Jones (LJ) potential,

$$U_{LJ}(r) = \begin{cases} 4\varepsilon \left[\left(\frac{\sigma}{r}\right)^{12} - \left(\frac{\sigma}{r}\right)^6 \right] & r \leq r_c \\ 0 & r > r_c \end{cases} \quad (3)$$

where ε and σ are the LJ units of energy and length and the cutoff $r_c = 2.5\sigma$. The monomer-monomer interaction ε is used as the reference and all monomers have the same diameter σ . For bonded monomers, we apply an additional potential where each bond is described by the FENE potential [20] with $k = 30 \varepsilon/\sigma^2$ and $R_0 = 1.5 \sigma$. The substrate is modeled as a flat surface since it was found previously [13] that with the proper choice of thermostat, the simulations using a flat surface exhibit the same behavior as a realistic atomic substrate with greater computational efficiency. The interactions between the surface and the monomers in the droplet at a distance z from the surface are modeled using an integrated LJ potential with the cutoff set to $z_c = 2.2\sigma$ [13]. Extending the range of this surface interaction to infinity increases the spreading rate of the precursor foot and slightly increases the spreading rate of the bulk. Aside from shifting the wetting transition to a lower energy, the qualitative spreading behavior is identical to the $z_c = 2.2\sigma$ case. Specifically, the absence of terraced wetting is probably not due to the finite interaction range of the surface used in simulations but to the length of the simulations. Here we present results for $\varepsilon_w = 2.0 \varepsilon$ which for $N = 10$ is above the wetting transition $\varepsilon_w^c = 1.75 \varepsilon$.

We apply the Langevin thermostat to provide a realistic representation of the transfer of energy in the polymer droplet. The Langevin thermostat simulates a heat bath by adding Gaussian white noise and friction terms to the equation of motion,

$$m_i \frac{d^2 \mathbf{r}_i}{dt^2} = -\Delta U_i - m_i \gamma_L \frac{d\mathbf{r}_i}{dt} + \mathbf{W}_i(t), \quad (4)$$

where m_i is the mass of monomer i , γ_L is the friction parameter for the Langevin thermostat, $-\Delta U_i$ is the force acting on monomer i due to the potentials defined above, and $\mathbf{W}_i(t)$ is a Gaussian white noise term. Coupling all of the monomers to the Langevin thermostat would have the unphysical effect of screening the hydrodynamic interactions in the droplet and not damping the monomers near the surface stronger than those in the bulk. To overcome this, we use a Langevin coupling term with a damping rate that decreases exponentially away from the substrate [21]. We choose the form $\gamma_L(z) = \gamma_L^s \exp(\sigma - z)$ where γ_L^s is the surface Langevin coupling and z is the distance from the substrate. In this paper, we present results

for $\gamma_L^s = 3.0$ and $10.0 \tau^{-1}$. The larger γ_L^s corresponds to an atomistic substrate with large corrugation and hence large dissipation and slower diffusion near the substrate.

For Pb on Cu(111), interactions are described via embedded atom method (EAM) interatomic potentials wherein the energy for N atoms is [22]

$$E = \sum_{i=1}^N [F_i(\rho_i) + \frac{1}{2} \sum_{j \neq i} \phi_{ij}(r)]. \quad (5)$$

In Eq. 5, ρ_i is the electron density at atom i , $\rho_i = \sum_{j \neq i} \rho_j^a(r)$, where $\rho_j^a(r)$ is the spherically symmetric electron density contributed by atom j , a distance r from i . $F_i(\rho_i)$ is the energy associated with embedding atom i into an electron density ρ_i and $\phi_{ij}(r)$ is a pair potential between atoms i and j . The many-body nature of $F_i(\rho_i)$ in Eq. 5 makes the EAM superior to pair potentials for describing bonding in metal systems. The interactions for Cu, Pb, and the cross-term between them were previously parameterized [23, 24, 25]. The Cu(111) substrate was described via an explicit atom description with dimension in the surface normal direction equal to four times the potential cutoff $r_c = 5.5 \text{ \AA}$. The substrate was equilibrated at the proper lattice constant prior to joining with the drop. Atoms in the $2r_c$ planes furthest from the surface are held rigid and the rest are permitted to relax according to MD equations of motion throughout all simulations. Because the substrate is represented atomistically for Pb(l) on Cu(111), we thermostat only atoms in the substrate using a Nose-Hoover thermostat algorithm.

All of the droplets presented here are modeled as hemicylinders as described previously [8]. The system is periodic in the y direction with length L_y and open in the other two directions. This allows a larger droplet radius to be studied using the same number of monomers than in the spherical geometry. Polymeric droplets have initial droplet radii of $R_0 \cong 50, 80,$ and 120σ , cross-sectional areas $A \cong 2690, 7490,$ and $18\,200 \sigma^2$ and a total size $N \cong 200\,000, 350\,000,$ and $780\,000$ monomers, respectively, with $L_y = 60 \sigma$ for $R_0 \cong 50 \sigma$ and $L_y = 40 \sigma$ for $R_0 \geq 80 \sigma$. Pb(l) droplets are studied with $R_0 \cong 20, 30,$ and 40 nm , $A \cong 630, 1400,$ and 2500 nm^2 and $N \cong 55\,000, 122\,000,$ and $220\,000$ atoms in the drop, respectively, with $L_y = 27 \text{ \AA}$. In each case, keeping $L_y < R_0$ or $L_y \approx R_0$ suppresses any Rayleigh instability. The substrates for the three drop sizes in the Pb(l) on Cu(111) systems contained $N \cong 85\,000, 128\,000,$ and $170\,000$ Cu atoms.

The equations of motion are integrated using a velocity-Verlet algorithm. For polymer spreading, we use a time step of $\Delta t = 0.01 \tau$ where $\tau = \sigma \left(\frac{m}{\varepsilon}\right)^{1/2}$. The simulations are

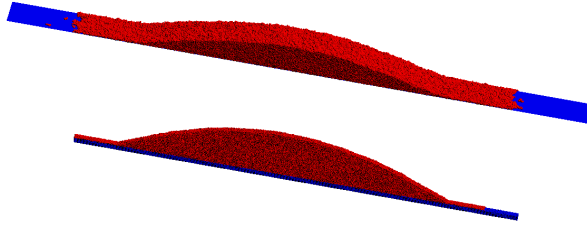


Figure 1: (color online) Cross-section snapshots from the simulations. A droplet composed of chain length $N = 10$ polymers with initial radius $R_0 = 80 \sigma$, thickness $L_y = 40 \sigma$, $\varepsilon_w = 2.0 \varepsilon$, and $\gamma_L^s = 3.0 \tau^{-1}$ at $t = 71600 \tau$ (top). A Pb(1) droplet with $R_0 = 40 \text{ nm}$ and $L_y = 27 \text{ \AA}$ on Cu(111) at $t = 3.6 \text{ ns}$ (bottom). The snapshots show substrates that are 750σ and 230 nm in length for the polymer and Pb droplets, respectively.

performed at a temperature $T = \varepsilon/k_B$ using the LAMMPS code [26]. For Pb(1) on Cu(111), $\Delta t = 1 \text{ fs}$, $T = 700 \text{ K}$, and the code PARADYN [27] was used.

For the polymeric system, it was shown previously [13] by measuring the equilibrium contact angle that finite system size effects become negligible for droplets containing 50 000 monomers or more. Here, we study the size dependence of the spreading behavior for droplets substantially larger than this finite size limit by using a minimum droplet size of 200 000 monomers in order to simultaneously study the bulk and precursor foot regions. This is shown in Fig. 1 which shows the foot extending beyond the bulk region. For the monomeric liquid system Pb on Cu(111), computational requirements for modeling the substrate are more significant so we use a minimum drop size $N \sim 55\,000$ atoms. In a prior work [28], wetting of Pb(1) drops on Cu(100) and Cu(111) was simulated using this model. For Pb(1) on Cu(111), a precursor film rapidly advanced ahead of the main drop in a diffusive manner (see Fig. 1); furthermore, the drop reached an equilibrium but finite contact angle $\theta_0 = 33^\circ$ on top of the prewetting film, which is in excellent agreement with experiment [28, 29, 30, 31]. This system exhibits negligible exchange of atoms between the liquid and solid, permitting evaluation of system size effects for non-reactive wetting in the case of a monomeric liquid with low vapor pressure.

For the simulations presented here, we extract the instantaneous contact radius $r_b(t)$ and contact angle $\theta(t)$ every 400τ for the polymer system and every 4 ps for the metal system according to the procedure described previously [8, 28]. To demonstrate the influence of the

viscous dissipation in the precursor foot on the dynamics of the bulk region, two systems are studied where the droplets are placed on substrates prewet with a monolayer of the same material to eliminate the simultaneous spreading of the precursor foot. The bulk contact radii for both a polymer droplet and a lead droplet are shown in Fig. 2 comparing spreading on prewet substrates to spreading on bare surfaces. Adding a monolayer to the substrate does not affect the bulk spreading for the polymeric system indicating that the viscous dissipation in the precursor foot is negligible for the droplet [32]. Although the Pb on Cu system is drastically different than the polymer system, the results are very similar. For the lead droplet, the early time behavior shows that the bulk spreading rate is enhanced as the foot is formed and begins to extend. Once the foot has extended away from the droplet, the bulk contact radius curves become parallel. Plotting the velocities of the precursor foot on both the bare and prewet surfaces shows that they are identical after one nanosecond.

The scaling predictions of the linearized kinetic and hydrodynamic models are applied to the bulk contact radius data for $\varepsilon_w = 2.0\varepsilon$ and $\gamma_L^s = 3.0$ and $10.0\tau^{-1}$ in Fig. 3a where dividing the bulk contact radius by $R_0^{4/5}$ for each of three droplet sizes causes the data to collapse to a single curve. The $R_0^{6/7}$ scaling of the same data, shown in Fig. 3b, does not fit as well because hydrodynamic energy dissipation has only a weak influence on the spreading rate for the conditions used in these simulations [8]. Similar results are found for Pb on Cu(111) (see Figs. 4a and b) because here we also have a low viscosity, rapidly spreading droplet.

Previous simulations of polymer droplet spreading [8] have shown that the hydrodynamic model, Eqs. 1 and 2 with $\zeta_0 = 0$, adequately fits the data only for the higher viscosity (longer chains) and slower spreading droplets. Here, a consistent improvement of the fit to the hydrodynamic model is observed for the three droplet sizes in going from the faster $\gamma_L^s = 3.0\tau^{-1}$ to the slower $\gamma_L^s = 10.0\tau^{-1}$ conditions as well as going from smaller to larger droplets. Both the kinetic and combined models fit the data well for all of the droplets although the combined model tends to produce less reasonable values of the fitting parameters [13].

The spreading of the precursor foot has been measured experimentally by ellipsometry and more recently by atomic force microscopy [17]. These studies report effective diffusion coefficients for the precursor foot without considering the dependence on the droplet size. Joanny and de Gennes predicted the height profile of the precursor foot to be proportional to $1/r$ [3, 33], but models relating the precursor foot dynamics to the droplet dimensions,

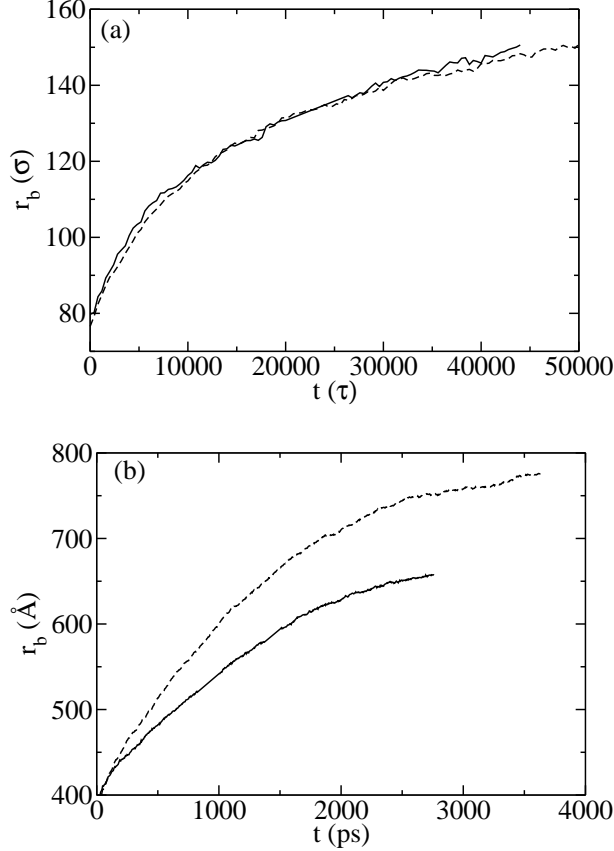


Figure 2: Comparison of bulk droplet spreading rate on prewet surface (solid line), and bare surface (dashed line) for (a) $N = 10$ polymers with $\varepsilon_w = 2.0\varepsilon$ and $\gamma_L^s = 10.0\tau^{-1}$ and (b) a Pb(l) droplet on Cu(111).

such as those presented above for the bulk dynamics, are not available. Like the results of the bulk contact radius, the size dependence is evident in the precursor foot contact radius as well. This is shown in Fig. 5 where the precursor foot contact radius is divided by the initial contact radius raised to the power n where $n = 1/2$. For the $\gamma_L^s = 10.0\tau^{-1}$ system, the curves in Fig. 5a show the same asymptotic behavior, but differences in the initial contact radius cause the curves to be offset by a constant value at later times. For the $\gamma_L^s = 3.0\tau^{-1}$ system, Fig. 5a shows the offset is less severe and the curves for the three different droplet sizes overlap. For Pb(l) on Cu(111), Fig. 5b shows results in this system are quite similar to what is seen for the $\gamma_L^s = 3.0\tau^{-1}$ case in the polymeric systems. This implies that Pb(l) on Cu(111) corresponds to a lower surface corrugation which, given the significant lattice mismatch between Pb and Cu and the high density packing of the (111)

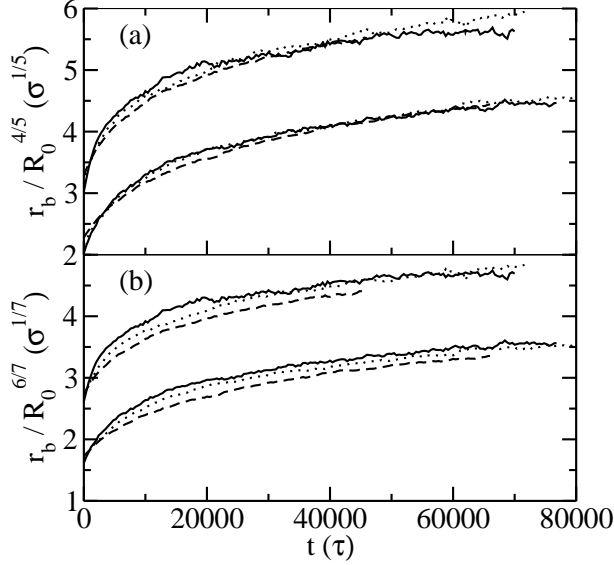


Figure 3: Scaling of the bulk contact radius for three droplet sizes based on the initial radii $R_0 = 50\sigma$ (solid line), $R_0 = 80\sigma$ (dotted line), and $R_0 = 120\sigma$ (dashed line) using the predictions of (a) the kinetic model and (b) the hydrodynamic model. Each droplet is composed of chain length $N = 10$ polymers with $\varepsilon_w = 2.0\varepsilon$, $\gamma_L^s = 3.0$ (upper curves) and $10.0\tau^{-1}$ (lower curves). The $\gamma_L^s = 3.0\tau^{-1}$ curves are shifted upward for clarity.

surface, is a reasonable result.

The precursor foot contact radius follows $r_f^2(t) = 2D_{eff}t$ where D_{eff} is the effective diffusion coefficient. Within the uncertainty of our data, these results are consistent with $D_{eff} \sim R_0^x$ where $x = 0.5 \pm 0.05$ even though the polymeric systems are completely wetting and the metal system is nonwetting. For the $\gamma_L^s = 10.0\tau^{-1}$ system, $D_{eff} \sim R_0^{0.65}$ collapses the data onto a master curve better than $R_0^{1/2}$. This may be due to the fact that the high coupling constant reduces the foot spreading rate to that of the bulk droplet, so the $D_{eff} \sim R_0^{1/2}$ scaling is not valid when the spreading of the bulk droplet interferes with the precursor foot diffusion. At present, there is no theoretical model we are aware of which predicts the dependence of D_{eff} on R_0 , but it may be because the higher bulk spreading rate of the larger droplets pushes the precursor foot outward adding to the driving force of the surface interaction.

In summary, we study the droplet size dependence of nanodroplets spreading in cylindrical geometries using molecular dynamics simulation. Our results follow the kinetic model of

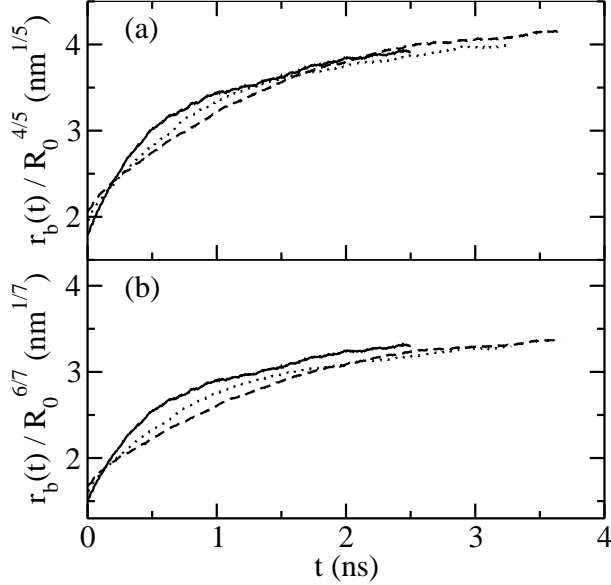


Figure 4: Scaling of the bulk contact radius of three Pb(l) droplet sizes based on the initial radii $R_0 = 20 \text{ nm}$ (solid line), $R_0 = 30 \text{ nm}$ (dotted line), and $R_0 = 40 \text{ nm}$ (dashed line) using the predictions of (a) the kinetic model and (b) the hydrodynamic model.

droplet spreading, which predicts a $R_0^{4/5}$ size scaling of the bulk droplet contact radius. The bulk spreading rate does not change if the droplet is instead spread on a prewet surface consisting of a monolayer of the droplet material. This indicates that, at least in the present simulations, the viscous dissipation from the precursor foot is not important for studying the kinetics of the droplet. Theories describing the dynamics of the precursor foot do not predict a droplet size dependence. The spreading rate of the precursor foot is known to be diffusive, but here we show that the effective diffusion coefficient has a droplet size dependence, $D_{eff} \sim R_0^{1/2}$, which can be utilized in the design of surface wetting applications. For Pb(l) on Cu(111), use of a realistic interatomic potential results in non-reactive wetting (in agreement with experiment). Furthermore, vapor pressure is low despite this being a monomeric liquid. As such, spreading mechanisms for the metal systems are similar to the polymeric systems studied and the same size dependence of the spreading rate is found despite the fact that these are two very different systems.

Sandia is a multiprogram laboratory operated by Sandia Corporation, a Lockheed Martin Company, for the United States Department of Energy's National Nuclear Security Admin-

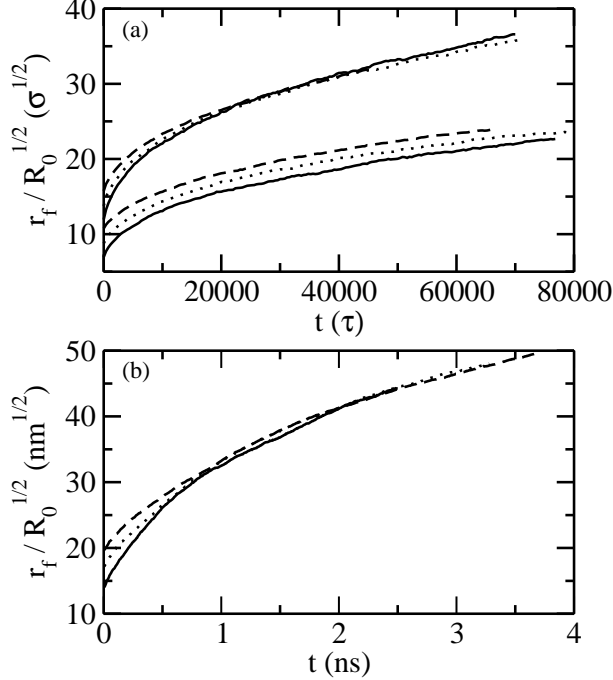


Figure 5: (a) Polymeric systems precursor foot spreading rate divided by $R_0^{1/2}$ for $R_0 = 50 \sigma$ (solid line), $R_0 = 80 \sigma$ (dotted line), and $R_0 = 120 \sigma$ (dashed line) for $\varepsilon_w = 2.0 \varepsilon$ and $\gamma_L^s = 10.0 \tau^{-1}$ (lower curves) and for $\gamma_L^s = 3.0 \tau^{-1}$ (upper curves). Each droplet is composed of chain length $N = 10$ polymers. The $\gamma_L^s = 3.0 \tau^{-1}$ curves have been shifted upward for clarity. (b) Precursor foot spreading rate for Pb(1) on Cu(111) divided by $R_0^{1/2}$ for $R_0 = 20, 30,$ and 40 nm at $T = 700 \text{ K}$.

istration under Contract No. DE-AC04-94AL85000.

-
- [1] F. Heslot, A. M. Cazabat, and P. Levinson, *Phys. Rev. Lett.* **62**, 1286 (1989).
 - [2] F. Heslot, A. M. Cazabat, P. Levinson, and N. Fraysse, *Phys. Rev. Lett.* **65**, 599 (1990).
 - [3] P. G. de Gennes, *Rev. Mod. Phys.* **57**, 827 (1985).
 - [4] F. Brochard-Wyart and P. G. de Gennes, *Adv. Coll. Interface Sci.* **39**, 1 (1992).
 - [5] S. Gladstone, K. J. Laidler, and H. J. Eyring, *The Theory of Rate Processes* (McGraw-Hill, New York, 1941).
 - [6] T. D. Blake and J. M. Haynes, *J. Coll. Interface Sci.* **30**, 421 (1969).
 - [7] M. J. de Ruijter, J. De Coninck, and G. Oshanin, *Langmuir* **15**, 2209 (1999).
 - [8] D. R. Heine, G. S. Grest, and E. B. Webb III, *Phys. Rev. E* **70**, 011606 (2004).

- [9] R. G. Cox, *J. Fluid Mech.* **168**, 169 (1986).
- [10] A. E. Seaver and J. G. Berg, *J. App. Poly. Sci.* **52**, 431 (1994).
- [11] M. J. de Ruijter, J. De Coninck, T. D. Blake, A. Clarke, and A. Rankin, *Langmuir* **13**, 7293 (1997).
- [12] S. Semal, T. D. Blake, V. Geskin, M. J. de Ruijter, G. Castelein, and J. De Coninck, *Langmuir* **15**, 8765 (1999).
- [13] D. R. Heine, G. S. Grest, and E. B. Webb III, *Phys. Rev. E* **68**, 061603 (2003).
- [14] T. D. Blake, A. Clarke, J. De Coninck, and M. J. de Ruijter, *Langmuir* **13**, 2164 (1997).
- [15] M. J. de Ruijter, T. D. Blake, and J. De Coninck, *Langmuir* **15**, 7836 (1999).
- [16] F. Heslot, N. Fraysse, and A. M. Cazabat, *Nature* **338**, 640 (1989).
- [17] H. Xu, D. Shirvanyants, K. Beers, K. Matyjaszewski, M. Rubinstein, and S. S. Sheiko, *Phys. Rev. Lett.* **93**, 206103 (2004).
- [18] J. A. Nieminen, D. B. Abraham, M. Karttunen, and K. Kaski, *Phys. Rev. Lett.* **69**, 124 (1992).
- [19] S. Bekink, S. Karaborni, G. Verbist, and K. Esselink, *Phys. Rev. Lett.* **76**, 3766 (1996).
- [20] K. Kremer and G. S. Grest, *J. Chem. Phys.* **92**, 5057 (1990).
- [21] O. M. Braun and M. Peyrard, *Phys. Rev. E* **63**, 046110 (2001).
- [22] M. S. Daw and M. I. Baskes, *Phys. Rev. B* **29**, 6443 (1984).
- [23] S. M. Foiles, M. I. Baskes, and M. S. Daw, *Phys. Rev. B* **33**, 7983 (1986).
- [24] H. S. Lim, C. K. Ong, and F. Ercolessi, *Surf. Sci.* **269/270**, 1109 (1992).
- [25] J. J. Hoyt, J. W. Garvin, E. B. Webb III, and M. Asta, *Modelling Simul. Mater. Sci. Eng.* **11**, 287 (2003).
- [26] S. Plimpton, *J. Comput. Phys.* **117**, 1 (1995).
- [27] S. J. Plimpton and B. A. Hendrickson, *Mat. Res. Soc. Proc.* **291**, 37 (1993).
- [28] E. B. Webb III, G. S. Grest, and D. R. Heine, *Phys. Rev. Lett.* **91**, 236102 (2003).
- [29] G. L. J. Bailey and H. C. Watkins, *Proc. Phys. Soc. London B* **63**, 350 (1950).
- [30] G. Prévot, C. Cohen, J. M. Guigner, and D. Schmaus, *Phys. Rev. B* **61**, 10393 (2000).
- [31] J. Moon, J. Lowekamp, P. Wybbblatt, S. Garoff, and R. M. Suter, *Surf. Sci.* **488**, 73 (2001).
- [32] In MD simulations of very small droplets, one can have a depletion effect where the drop spreading is effected by the transport of material to the precursor foot, but this is not one of the three dissipation mechanisms mentioned by de Gennes and is not relevant here.
- [33] J. F. Joanny, *Thesis, Université Paris VI* (1985).